Raman identification of CaCO3 polymorphs in concrete prepared with carbonated recycled concrete aggregates

M. Marchetti, G. Gouadec, M. Offroy, M. Haouchine, A. Djerbi, O. Omikrine-Metalssi, J.-M. Torrenti, J.-M. Mechling, G. Simon, P. Turcry, et al.

HAL Id: hal-04680626

https://hal.science/hal-04680626

Submitted on 28 Aug 2024

1 Raman identification of CaCO$_3$ polymorphs in concrete prepared with carbonated recycled
2 concrete aggregates
3
4

5 Marchetti M.[1], Gouadec G.[2], Offroy M.[3], Haouchine M.[3], Djerbi A.[1], Omikrine Metalssi O.[1],
6 Torrenti J.-M.[1], Mechling J.-M.[4], Simon G.[2], Turcry P.[5], Barthelemy P.[6], Amiri O.[7]
7
8 [1] Univ Gustave Eiffel, MAST, UMR MCD, 14-20 Boulevard Newton, Cité Descartes, Champs-
9 sur-Marne, F-77447 Marne la Vallée Cedex 2, France
10 [2] Sorbonne Université, CNRS, MONARIS (UMR 8233), c49, F-75252, Paris, France.
11 [3] Université de Lorraine, CNRS, LIEC, F-54000 Nancy, France
12 [4] Université de Lorraine, CNRS, IJL, F-54000 Nancy, France
13 [5] LaSIE, UMR CNRS 7356, La Rochelle Université, France
14 [6] CERIB, France
15 [7] GEM, Nantes University, France
16
17

Abstract

19 The urge to preserve natural resources, to reduce cement production CO$_2$ emissions and to recycle
20 concrete waste conducted to the French national program FastCarb. It is aimed at using recycled
21 concrete aggregates (RCAs), once carbonated with CO$_2$ coming from cement production sites, as
22 a replacement for natural aggregates. The carbonation step serves to reduce the porosity of the old
23 cement paste and to improve future concrete properties. Two different carbonation processes
24 (rolling drum (P1), fluidized bed (P2)) were tested and the resulting RCAs were mixed in different
25 weight proportions with natural aggregates to elaborate new concretes. Raman investigations were
26 then conducted on some sections to analyze the carbonated phases and their spatial distribution.
27 Results indicated a difference in polymorphs distributions. Process P1 seems to generate more
28 vaterite than process P2, which mainly generates calcite and aragonite. They also allowed to
29 appreciate the thickness of the interface between the old and the new cement pastes.
30
31

Highligths

33 • Two accelerated carbonation processes were used at an industrial scale to clog the porosity of
34   the old cement past present on recycled cement aggregates (RCAs)
35 • Raman spectroscopy was implemented to determine the distribution of CaCO$_3$ polymorphs in
36   carbonated RCAs and the interfacial zone between the old and new cement pastes
37 • Results indicated the nature of polymorphs changed depending on the carbonation process
38
39

40 **Keywords**: CO$_2$ intake, carbonation, CaCO$_3$ polymorphs, Raman spectroscopy, chemometrics
41
42

Introduction

44 Concrete remains one of the most used building materials in the world (even more than steel) and
45 the global cement production was about 4.1 billion tons in 2019 [1]. Portland cement (PC) is the
46 traditional binder for concrete and its production generates 1 ton of CO$_2$ per ton. Cement
47 industries are thus responsible for 7% of the world's total CO$_2$ emissions and the International
48 Panel on Climate Change (IPCC) reports direct CO$_2$ emissions from carbonates in cement
49 production to be around 4% of the total fossil CO$_2$ emissions (1.6 % in France) [2]. Several
50 sustainability plans aimed at trapping this greenhouse gas and avoiding its accumulation into the
51 atmosphere, have thus been announced, such as the Industrial Deep Decarbonization Initiative

(IDDI) [3]. Furthermore, there is a growing policy to promote the use of recycled concrete aggregates (RCAs) and therefore preserve natural resources [4-10]. Yet, RCAs are more porous than natural aggregates, which affects the resulting concrete properties [11-17]. RCAs properties need to be improved to qualify for substitution, starting with their porosity. Several laboratory studies have shown that carbonation improves the characteristics and the quality of RCAs, clogging their porosity with the mineralization of CO_2 [18-27], although some inhomogeneities were observed [28] and modelled [29]. These elements drove to the development of RCA accelerated carbonation processes, both at the laboratory scale [8-10] and, within the FastCarb project, at an industrial scale [27, 30]. Some questions were nevertheless raised about the nature of $CaCO_3$ polymorphs and their spatial distribution in carbonated RCA alone and once included in concrete. Several studies have shown that accelerated carbonation could induce the formation of different $CaCO_3$ polymorphs, i.e. portlandite, vaterite, aragonite or amorphous [31-33]. Their distribution is obviously affected by the CO_2 concentration [34], and a 3% CO_2-enriched atmosphere tended to promote the precipitation of the vaterite and aragonite with regards to calcite. But other properties of the environment [35] such as temperature [36], that did not promote aragonite and vaterite presence, and pH [37] also influences the properties of the carbonated concrete [38].

Many analytical techniques do exist to characterize carbonated phases, starting with the phenol phthalein test, X-ray diffraction (XRD), thermogravimetric analysis (TGA), or EDX-coupled scanning electron microscopy (SEM). These tests are destructive and time-consuming. Haque et al. introduced several non-destructive alternatives, among which Raman spectroscopy [39], though not presented as the most appropriate. This technique was first used as early as in the mid-seventies [40, 41] but there are very few later reports on the Raman spectroscopy detection of carbonated phases in cementitious materials [42-46], especially when one considers the abundant literature on the subject. Raman spectroscopy has also recently been successfully implemented to monitor both the cement paste hydration and the carbonation of portlandite, the stability of single phase C3A hydrates [47-52].

The objective of this research is to use Raman spectroscopy to detect and identify $CaCO_3$ polymorphs in RCAs and ultimately to map their distribution, both in their pristine carbonated state and once included in concrete samples. Investigations will focus on the influence of the carbonation process and the thickness of the interfacial transition zone between the new cement paste and the old one found in the RCAs.

Materials and methods

Carbonation processes, and recycled concrete aggregates (RCAs)
Two distinct carbonation processes were considered, both operating at an industrial scale, and details are provided by Torrenti et al. [27]. One used a rolling drum dryer (Vicat pilot plant, in Créchy (France)), and the other used a fluidized bed dryer (Holcim Val d' Azergues cement plant (France)). In both cases, the recycled material was exposed to gases from a cement plant, with a CO_2-content of close to or over 15 % in volume, at around 70°C [30]. These conditions were prone to trigger accelerated carbonation, the CO_2 concentration in the atmosphere being of 400 ppm. The main other differences between the processes do consist in percentage of CO_2 (between 11% and 16% for the drum, while of about 20% for the fluidized bed) and the temperature (between 40°C and 60°C for the drum, while it is near 70°C for the fluidized bed).

RCAs from these industrial productions did contain an unavoidable old cement paste, coming from destructed buildings and infrastructures, which composition was totally unknown. RCAs diameters were below 14 mm which is adapted to the elaboration of new concretes. RCAs with a diameter below 2 mm were considered as sand (S) while those with a larger diameter were considered as gravel (G).

Concrete samples elaborated with RCAs

Seven concretes were elaborated with varying weight proportions of natural aggregates (N), uncarbonated RCAs (URCA), and carbonated RCAS (CRCAs) prepared in either the rolling drum (P1) or the fluidized bed dryer (P2) – see Table 1- and as described by Torrenti et al. [27]. The carbonation status of CRCAs is unknown and the purpose of this study is to also to identify the thickness of the carbonated zone in addition to the spatial repartition of $CaCO_3$ polymorphs.

	sand (S) fraction (% w/w)				gravel (G) fraction (% w/w)			
	NS	URCAS	CS_P1	CS_P2	NG	URCAG	CRCAG_P1	CRCAG_P2
concrete 1	100				100			
concrete 2	80	20			50	50		
concrete 3	80		20		50		50	
concrete 4	80			20	50			50
concrete 5	60	40				100		
concrete 6	60		40				100	
concrete 7	60			40				100

Table 1: Aggregates contents and types of concretes considered in this study

C25 concrete samples were 4 cm x 4 cm x 16 cm parallelepipeds. They were obtained by mixing aggregates with CEM II/A cement and water, with a water to cement ratio of 0.55 in each case. The aggregates were saturated with water before mixing with other constituents to avoid to affect the selected water to cement ratio, considering the results from Sereng et al. [26]. The size of the concrete samples is large enough to avoid any incidence on the interfacial zone (ITZ) [51] between the old cement paste present on RCA and the new paste.

Once the setting was completed, three prismatic samples of 4 cm x 4 cm section and roughly 2 cm-thickness were sawn without water, then coated with a resin. Prismatic samples were chosen to ease further spectroscopic analysis in terms of sample size. The surface with the 4 cm x 4 cm section was then polished, first with grinding disks (220 and 1200 grades), and then with diamond powder (9, 3, and 1 μm), in all cases using ethanol (Normapur grade, purity over 99.8%). Polished samples were then stored in sealed plastic bags before spectroscopic analysis to prevent the surface for further carbonation.

Raman spectrometry and spectra pre-processing

Raman spectroscopy measurements were obtained with a HR800 LabRam spectrometer (Horiba Scientific, Jobin-Yvon), using the 514 nm laser line of an Argon ion laser (Coherent). This wavelength (or a close one) is commonly used with cementitious materials, in spite of some fluorescence issues [50, 55-58]. The spectrometer is coupled with a BX Olympus microscope and we used a x50 (NA 0.75) MPlanN objective, from Olympus "UIS-2" series. This gave an estimated diffraction-limited spot size of about 1 μm. Both in-line profiles and 2D-mappings were recorded with 1 to 5 μm displacement steps of the XY-motorized stage. The combination of a 600 grooves/mm grating and an Ultra Low Frequency "ULF" module gave access to the ~40 – 1800 cm^{-1} range in a single window. This way we had access to the usual spectral peaks (around 710 and 1080 cm^{-1}) but also to low frequency lattice modes allowing for full differentiation of $CaCO_3$ polymorphs [59, 60]. The laser power was set to measure 1 mW on the sample and the integration time was set between 5 and 20 s (depending on the sample), each measurement starting after prior 10 s photobleaching. Each spectrum was treated for spikes removal, baseline-corrected by a 5th-order polynomial function and normalized with respect to the maximum intensity peak in the 1080-1090 cm^{-1} region.

Figure 1: A concrete sample observed with a x10 objective to prepare a mapping, the white light spot being focused on the interface between the old paste (lighter) and the new one (darker)

144
145 Spectroscopic observations were specifically performed at the interface between the old cement
146 paste present in the RCAs and the new one used to elaborate the concrete samples. The choice of
147 the investigation zones was performed through a three-step sequence:
148   i)   the visual detection of the interface (Figure 1),
149   ii)   a microscope observation with a x10 magnification,
150   iii)   the selection of the specific zone to be analyzed with a x 50 magnification (Figure 2).
151 Each selected zone was assumed to be representative of the investigated sample.
152
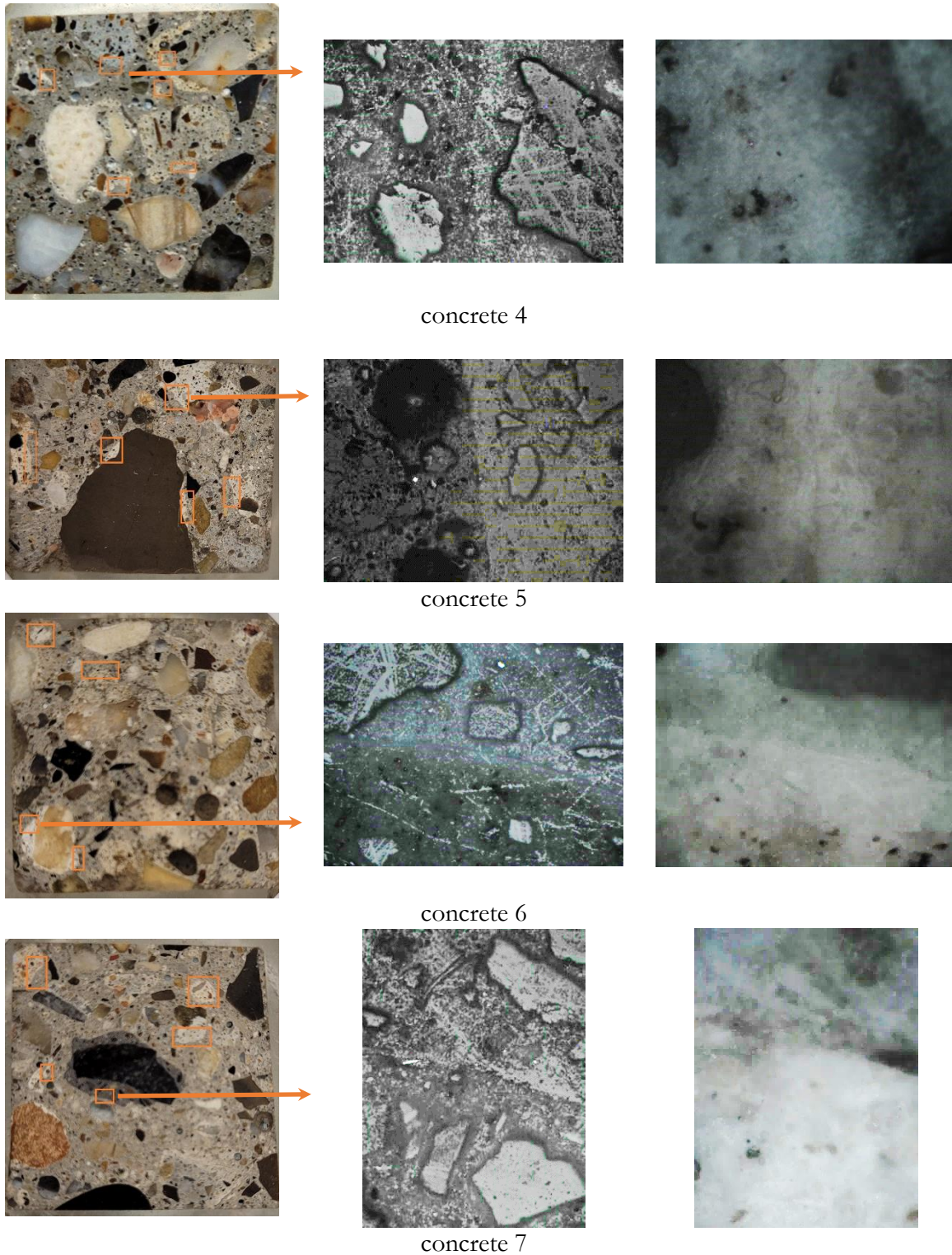
Figure 2: Pictures of some polished concrete sections obtained with a digital color camera (left column) or through x10 (middle column) and x50 (right column) microscope objectives. They all exhibit the frontier between the old cement paste (brighter) and the new one (darker).

154

Chemometrics analysis

155 *Chemometrics analysis*

156 Chemometrics is the science dedicated to the extraction of the most relevant information from a
157 set of experimental data [61, 62], including from physico-chemical and spectroscopic
158 measurements [63, 64]. It has been successfully used in many research fields [65] to acquire a better
159 knowledge of the analyzed samples, including in Raman imaging [63]. Chemometrics tools have
160 recently been applied to Raman spectra of civil engineering materials [48, 49, 51]. In this study,
161 principal components analysis (PCA) and Multivariate Curve Resolution - Alternating Least
162 Squares (MCR-ALS) methods were applied to the Raman spectra. In particular, MCR-ALS is able
163 to extract Raman spectra of specific pure materials which are mixed into collected Raman spectra.
164 In the specific case of $CaCO_3$ polymorphs, their Raman signature being different, the MCR-ALS
165 should be able to extract them from the collected spectral data collected on carbonated RCA
166 samples. Several preprocess approaches could be used to correct raw data before the initialization
167 step of the MCR-ALS algorithm. Two specific preprocess approaches were then compared in this
168 paper. The first one is (i) spikes removal, (ii) a simple baseline correction with a polynomial and
169 (iii) a min-max normalization. The second one is (i) spikes removal, (ii) a baseline correction by
170 Weighted Least Squares (WLS), (iii) a normalization L1 and (iv) a recently developed algorithm
171 called MT-SVD which handles rank deficiency and noise [67], based on effective truncated
172 singular-value decomposition (MT-SVD). In the rest of the paper and for greater clarity, these two
173 types of correction were respectively designated as PP1 and PP2. In both cases, during the
174 initialization step of the MCR-ALS, the SIMPLe-to-use Interactive Self-Modelling Mixture Analysis
175 (SIMPLISMA) was applied [68-70]. MATLAB R2016a was used for all computer calculations.
176 The objective of the chemometrics analysis is to de-mix the spectral response and identify the
177 spatial distribution of CaCO3 polymorphs at the interface between the old cement paste (present
178 in the RCAs) and the new paste of each sample.

179

180 **Results and discussion**
181 *$CaCO_3$ polymorphs identification*
182 A selection of PP1-corrected Raman spectra of the old cement paste on RCA from concrete 1, 5,
183 6 and 7 is given in Figure 3. Spectra are over the 40-1200 cm^{-1} spectral range, with the indexation
184 of $CaCO_3$ polymorphs based on the literature [48, 50, 51, 71-82]. The spectra are very similar from
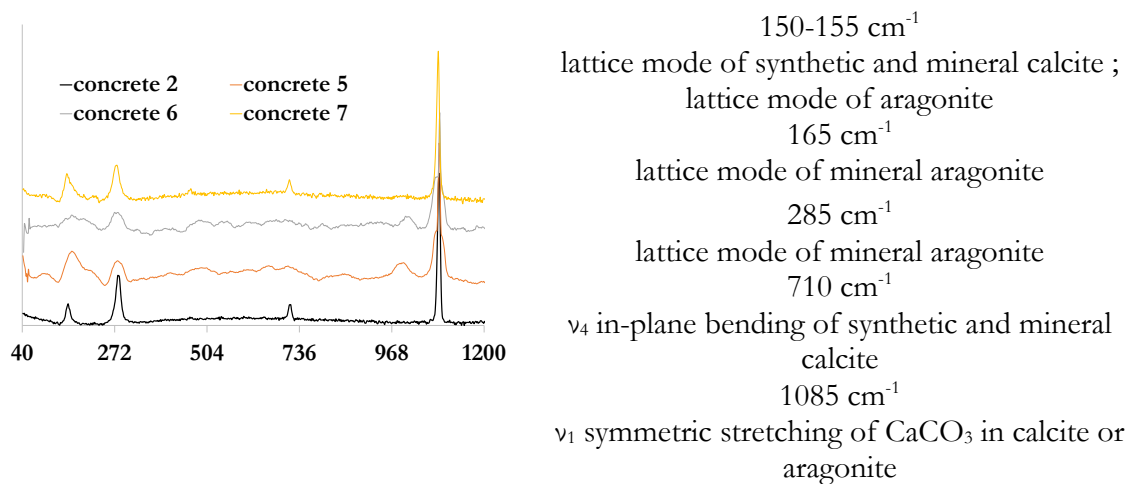185 one sample to another and it is difficult to observe selective peaks of $CaCO_3$ polymorphs.

186

150-155 cm^{-1}
lattice mode of synthetic and mineral calcite ;
lattice mode of aragonite
165 cm^{-1}
lattice mode of mineral aragonite
285 cm^{-1}
lattice mode of mineral aragonite
710 cm^{-1}
ν_4 in-plane bending of synthetic and mineral
calcite
1085 cm^{-1}
ν_1 symmetric stretching of $CaCO_3$ in calcite or
aragonite

Figure 3: Selected normalized Raman spectra obtained on polished surfaces of RCA-containing
concretes 2, 5, 6 and 7 (λ_{laser} = 514 nm, x50 magnification. The spectra were offset for clarity).

187

188 *Identification and thickness of the interfacial transition zone (ITZ) between old and new cement pastes*

A preliminary identification of the number of chemical species and their nature relied on a Principal Component Analysis. The results of a PCA on PP2-corrected Raman spectra (Figures 4a and 4b) indicated that no more than three components could be identified with a potential spectral meaning, explaining nearly 80% of the variance. These components are close to the spectral signature of calcite, as illustrated in Figure 4c.
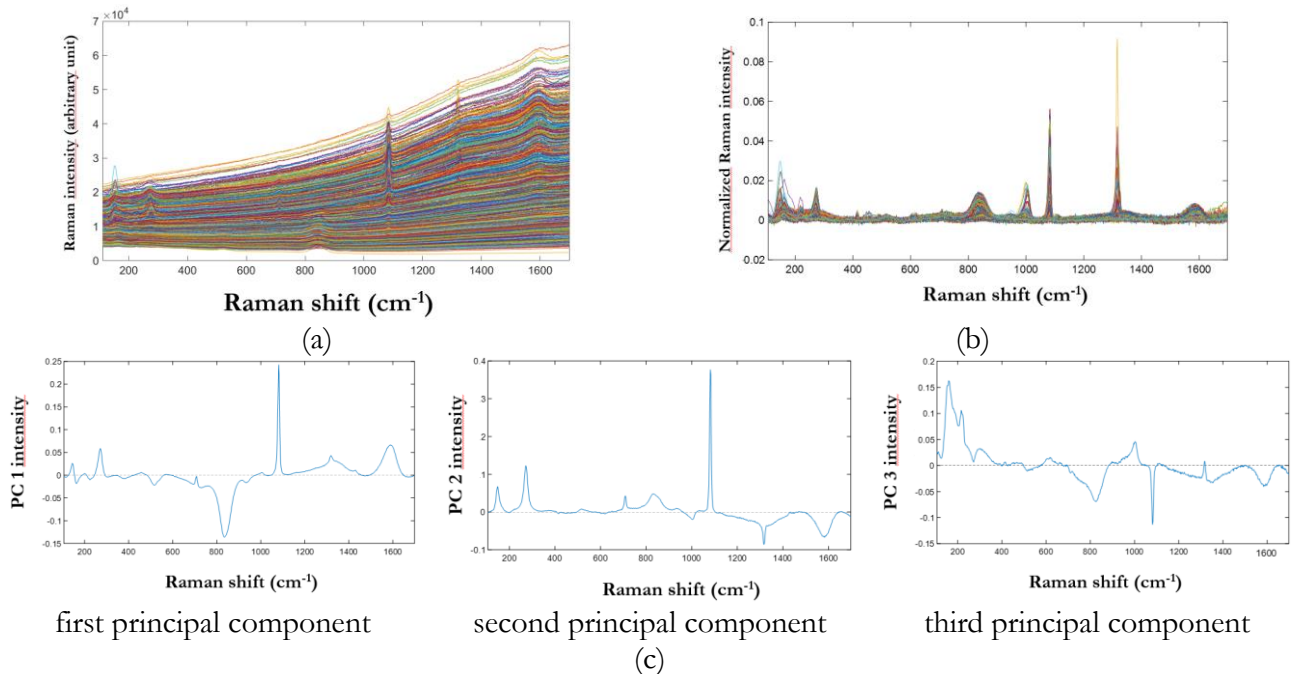

	(a)		(b)

first principal component	second principal component	third principal component

(c)

Figure 4: Raw Raman data obtained with a sample of concrete #7 containing RCAs (a),
PP1-corrected Raman data (b), and first three principal components
with the specific peak of carbonate near 1085 cm^{-1} (c)

Raman line-profiles were recorded going across the old and the new cement pastes interface, regardless of the carbonation process (P1 or P2). These profiles lengths ranged between 80 and 140 μm. After being preprocessed, Raman profiles were treated by MCR-ALS initialized by SIMPLISMA, with non-negativity and unimodality constraints, so as to identify to what extent Raman spectra of calcite, aragonite, and vaterite could be extracted and their distribution quantified. The spectral range upon which calculations were performed depended on the specific spectral acquisition window but always remained below 1300 cm^{-1}. The results are presented in Figure 5. Calcite was observed in all concrete samples, which was expected, and aragonite was never detected. This is consistent with the results of Xue et al. [53] indicating aragonite is usually not detected under low CO_2 pressure. In this case, the temperature rise of selected processes did not trigger a specific growth of this polymorph in all samples. Vaterite was only detected once, in concrete 3, which is consistent with the presence of carbonated RCA (CRCA). In this case, the vaterite concentration does not reach a maximum value, contrary to calcite. This aspect is a first indication that carbonation processes P1 and P2 have an incidence on polymorphs distribution. A specific focus was brought to the Interfacial Transition Zone (ITZ) between the two different pastes in the samples of concrete 2 and 3. The old cement past was visually identified by visual observation and before Raman mapping. It was assumed that the interface with the carbonated zone extends between the point where calcite concentration drops significantly and the point where another chemical is detected. Results are illustrated in Figure 6. It appears that the ITZ roughly is 20 μm-thick, although in one case the profile is not orthogonal to the interface between the two cement pastes. This value is consistent with results published by Djerbi [54].

217 Nevertheless, such an approach did not allow to identify with a sufficient degree of confidence the
218 presence or the absence of $CaCO_3$ polymorphs. Therefore, 2D-mappings were specifically
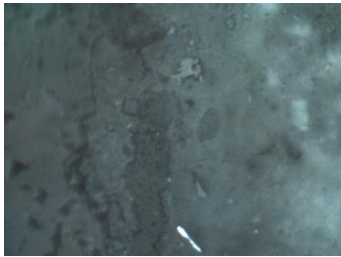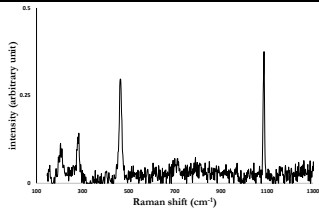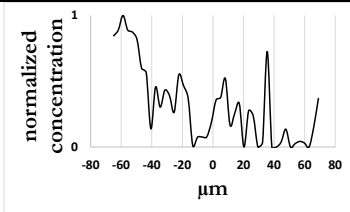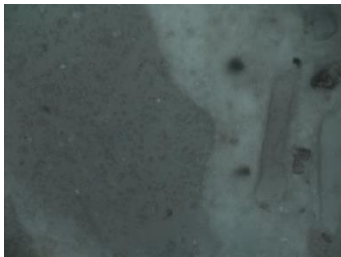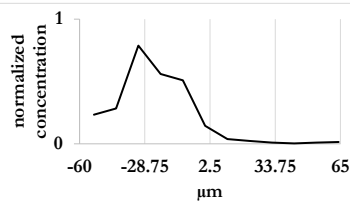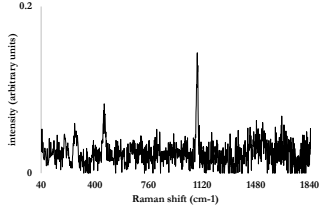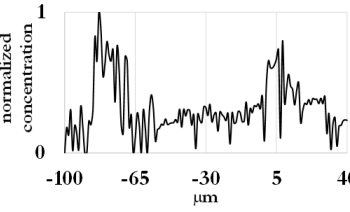219 performed on some concretes containing carbonated RCAs.
220
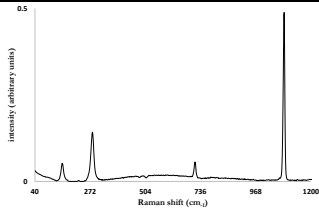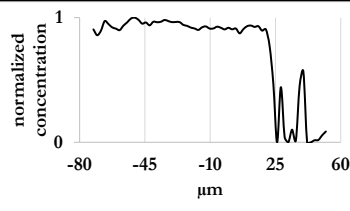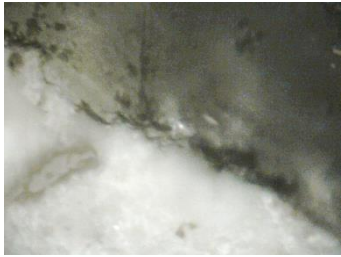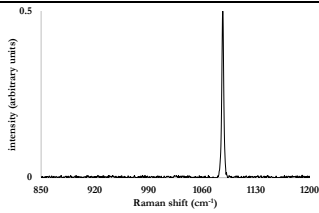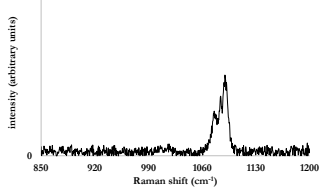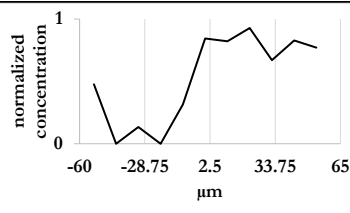
Concrete	Picture of the analyzed zone	$CaCO_3$ polymorphs extracted by MCR-ALS (from top to bottom: calcite, aragonite, and vaterite)	Concentrations of the $CaCO_3$ polymorphs extracted by MCR-ALS
# 1		aragonite not extracted vaterite not extracted	
# 2		aragonite not extracted vaterite not extracted	
# 3		aragonite not extracted	
# 4		aragonite not extracted vaterite not extracted	

Figure 5 (part 1): Pictures of the interface between the old cement paste of a RCA and the new cement paste in a concrete containg carbonated RCA (2nd column), spectra of identified $CaCO_3$ polymorphs (3rd column) and their respective concentrations (4th column) after a SIMPLISMA and a MCR-ALS on collected and processed Raman spectra
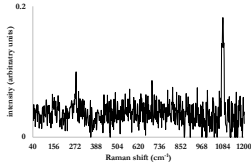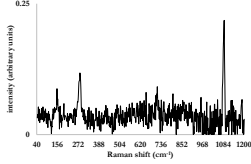
221
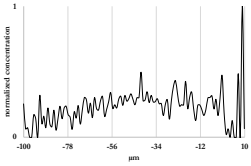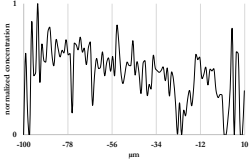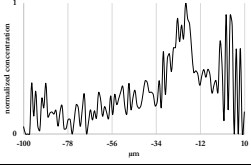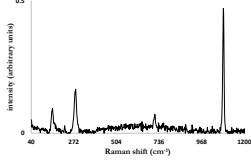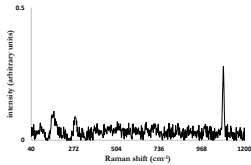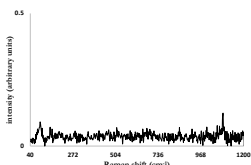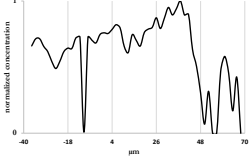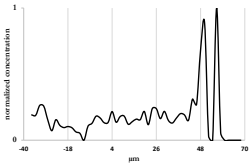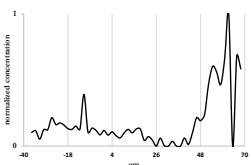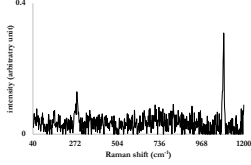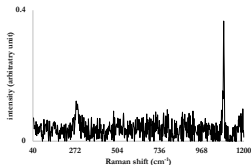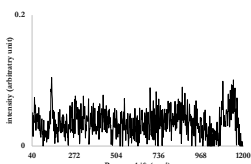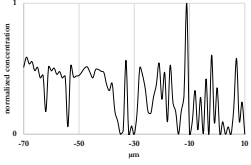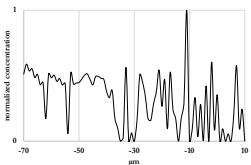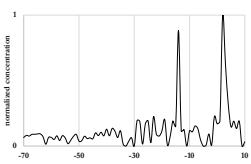
Concrete	Picture of the analyzed zone	CaCO₃ polymorphs extracted by MCR-ALS (from top to bottom: calcite, aragonite, and vaterite)	Concentrations of the CaCO₃ polymorphs extracted by MCR-ALS
# 5			
#6			
# 7			

Figure 5 (part 2): Pictures of the interface between the old cement paste of a RCA and the new cement paste in a concrete containing carbonated RCA (2nd column), spectra of identified CaCO₃ polymorphs (3rd column) and their respective concentrations (4th column) after a SIMPLISMA and a MCR-ALS on collected and processed Raman spectra
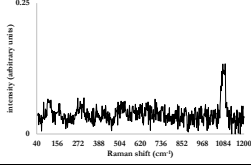
concrete 2
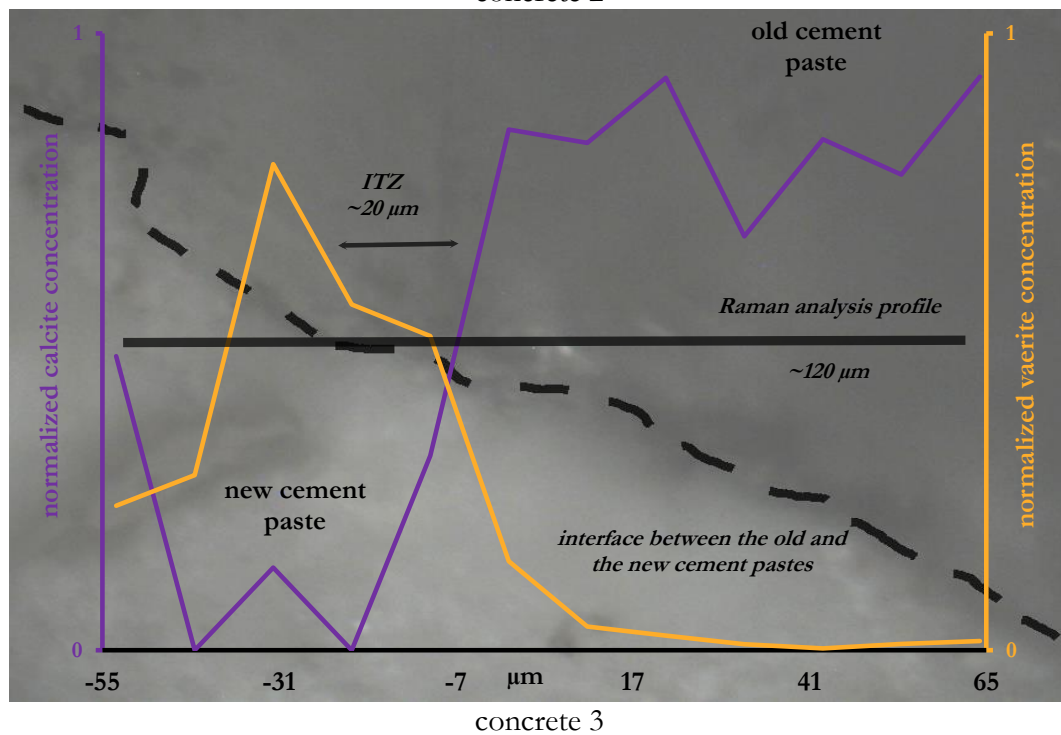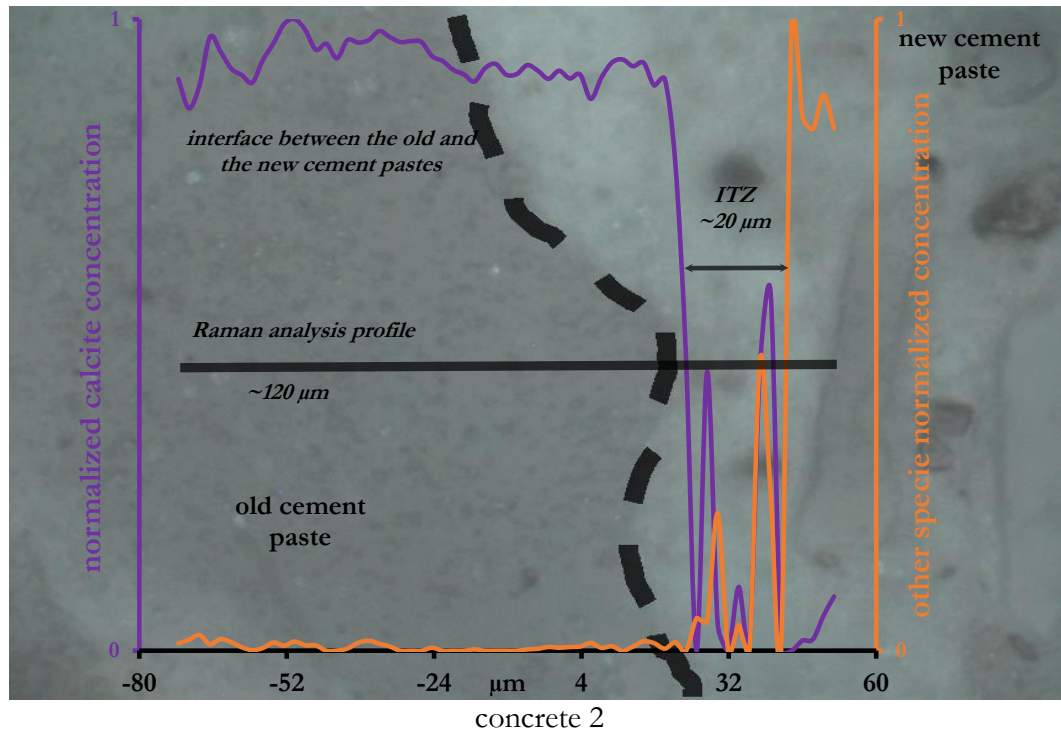
concrete 3

Figure 6: Concentrations of calcite and vaterite detected across the interface between the old and new cement pastes in concrete #2 (upper graph) and concrete #3 (lower graph) samples containing carbonated RCAs. The curves were obtained from pre-processed Raman spectra after SIMPLISMA and MCR-ALS procedures. A double arrow shows the estimate of the Interfacial Transition Zone (ITZ) thickness.

225 *Mapping of the CaCO₃ polymorphs and corresponding spatial distributions*
226   The spatial distribution of $CaCO_3$ polymorphs was specifically investigated in concretes 4, 6, and
227 7, which all contained carbonated RCAs. The aim was to establish the differences between the two
228 carbonation processes and investigate how the old cement paste interacted with the new one.
229 Hyperspectral images were obtained by analyzing an interface between the two cement pastes by
230 micro-Raman spectroscopy, with a x50 objective lens. Results were preprocessed according to the
231 PP1 approach.
232   A SIMPLISMA initialization followed by MCR-ALS analysis with non-negativity and unimodality
233 constraints was conducted over the 40-1200 cm^{-1} range. The distributions of polymorphs that could
234 be extracted are presented in Figure 7. The concentration of each polymorph was normalized over
235 the studied area, which ranged between a few hundreds of μm^2 to slightly above one thousand of
236 μm^2. All polymorphs are present in the two samples with RCA carbonated according to process
237 P2 (concretes 4 and 7), while mainly calcite and vaterite are present in the RCA of concrete 6,
238 which was carbonated according to process P1. In this concrete, the proportion of all polymorphs
239 seems to be balanced. In the case of concrete 7, the spectral signature attributed to calcite (peaks
240 at 712 and 1085 cm^{-1}) does contain peaks that can be attributed to aragonite (153 and 285 cm^{-1}),
241 revealing an incomplete de-mixing process. The chemometrics approach also revealed a spectral
242 signature that can be attributed to gypsum (peak at 1008 cm^{-1}).

244   Because some of the spectral measurements are noisy, and the question about the rank
245 determination (i.e. the number of chemical species to be extracted from the Raman hyperspectral
246 images) was still pending. Therefore, PP2-corrected Raman spectra was tested before MCR-ALS
247 implementation (Figure 8). This time, the calculations were conducted considering the full spectral
248 range of collected spectra (40-1800 cm^{-1}). The results obtained after both SIMPLISMA and MT-
249 SVD initializations seemed similar in the case of concretes 4 and 6. But some discrepancies
250 appeared in the case of concrete 7. The de-mixing consecutive to the MT-SVD option confirmed
251 the presence of gypsum but it was not fully efficient to discriminate calcite from aragonite, even
252 though the peaks that were identified seem to better correspond to aragonite (148 and 272, 708
253 cm^{-1}) than calcite (1088 cm^{-1}). It must also be noted that the PP2 correction did result in a greater
254 amount of calcite detected in concrete 6 (carbonation process P1) than with the PP1 correction.
255   In conclusion, a preprocess including MT-SVD does help the MCR-ALS algorithm to classify more
256 accurately which $CaCO_3$ polymorph was present in each concrete than a conventional preprocess
257 such as PP1. The carbonation process P1 seems to generate more vaterite than process P2, which
258 mainly generates calcite and aragonite. Although Raman spectroscopy is a local method, the
259 performed mapping and the representativity of the carbonated RCA corroborates this statement.
260 Furthermore, this result is consistent with the indication that polymorphs are generally observed
261 in carbonated samples when exposed to high CO_2 concentration [33].
262
263

	concrete #4 (P2 carbonation process)	concrete #6 (P1 carbonation process)	concrete #7 (P2 carbonation process)
calcite spatial distribution			
aragonite spatial distribution			
vaterite spatial distribution			
gypsum spatial distribution	not detected	not detected	

Figure 7: 2D-spatial normalized distribution of $CaCO_3$ polymorphs, as obtained by MCR-ALS (non-negativity and unimodality constraints, 40-1200 cm-1 spectral range) performed after a SIMPLISMA initialization on PP1-corrected Raman maps containing both the old and the new cement pastes.

264

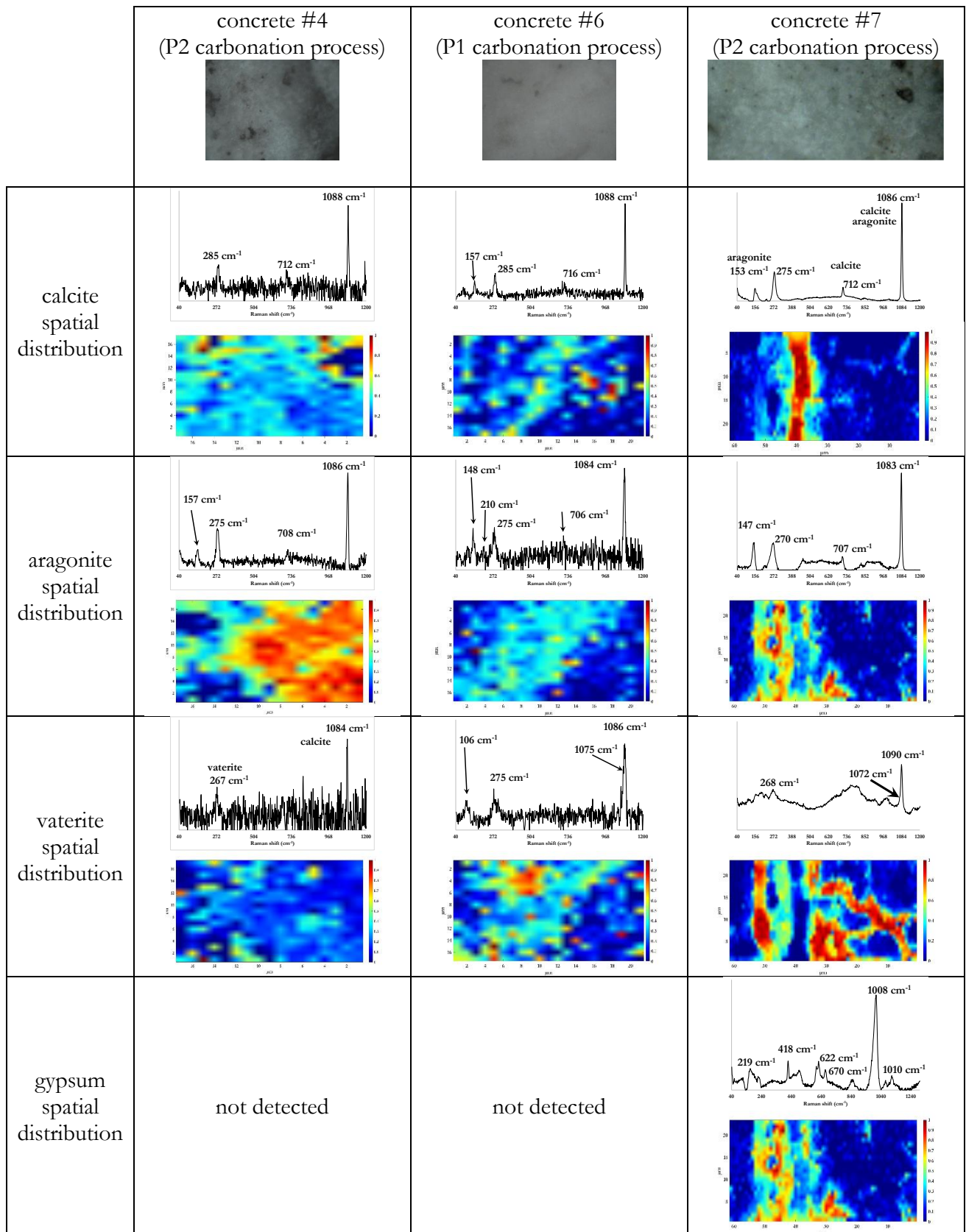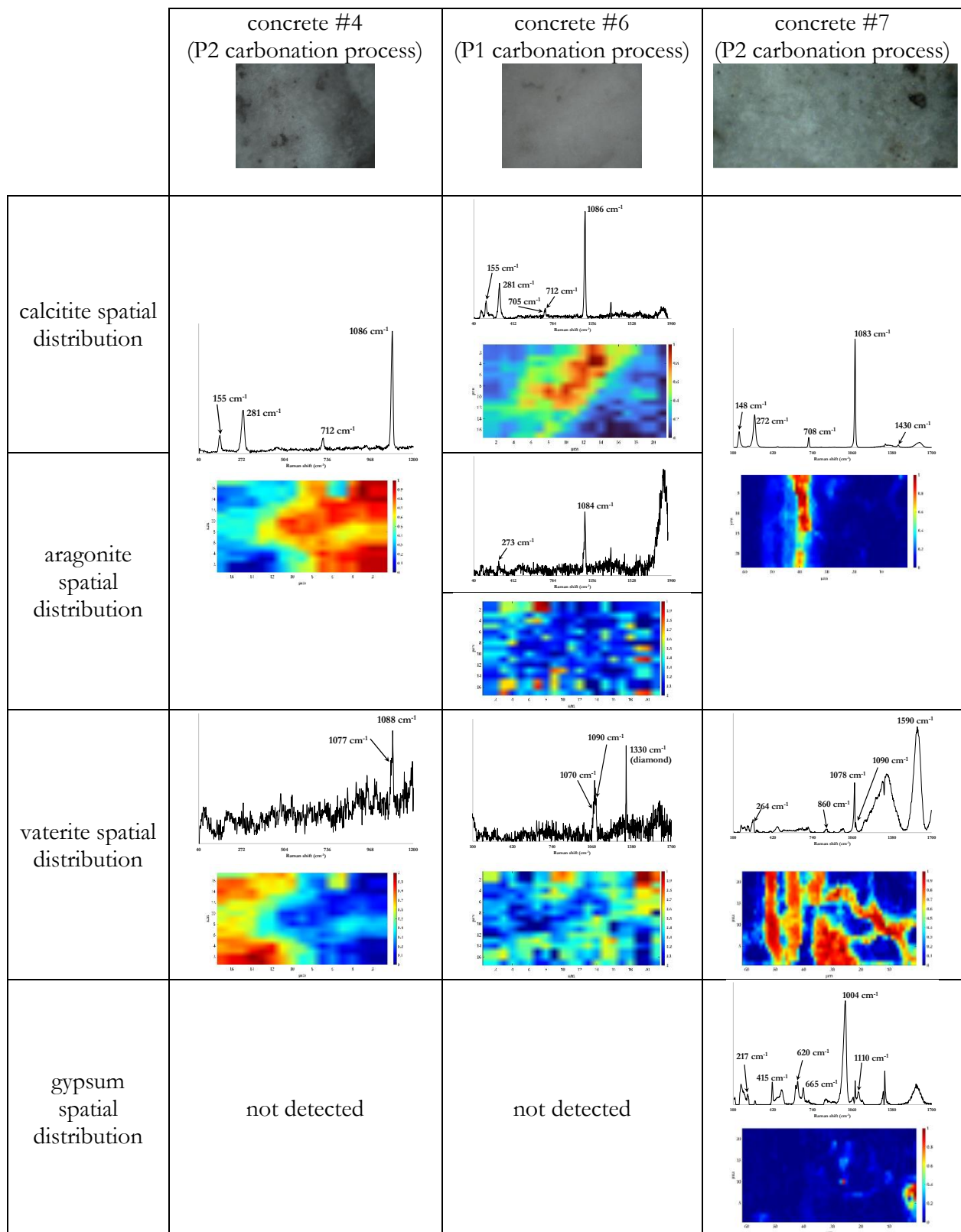|	concrete #4 (P2 carbonation process)	concrete #6 (P1 carbonation process)	concrete #7 (P2 carbonation process)
calcitite spatial distribution			
aragonite spatial distribution			
vaterite spatial distribution			
gypsum spatial distribution	not detected	not detected	

Figure 8: 2D-spatial normalized distribution of $CaCO_3$ polymorphs, as obtained by MCR-ALS (non-negativity and unimodality constraints, 40-1200 cm-1 spectral range) performed after a SIMPLISMA initialization on PP2-corrected Raman maps containing both the old and the new cement pastes.

265
266

Conclusion

Concrete aggregates recycled from the demolition of buildings and infrastructures (RCAs) are considered as a potential substitute for natural aggregates. Their microstructural properties need to be improved for RCA concrete to comply with standard mechanical requirements. A project was developed to trap CO2 emitted by cements industries to chemically modify the RCAs and block their porosity (by means of carbonation), and is very promising. The process was implemented at an industrial scale and in an accelerated way (natural carbonation is a slow process). The resulting samples were later analyzed by Raman spectroscopy. This technique confirms previous reports that the interfacial transition zone (ITZ) between a new cement paste and the old one (from carbonated RCAs) is around 20 μm wide. It was also able to discriminate $CaCO_3$ polymorphs (calcite, aragonite, and vaterite) and to identify which one is predominantly generated depending on the two tested carbonation processes (rolling drum dryer vs. fluidized bed dryer). Coupled with chemometrics tools, the spatial repartition of each polymorph was obtained either on linear profiles or on mappings. The incidence of $CaCO_3$ polymorphs and of carbonation process on porosity clogging needs a specific investigation, along with their ones on the compressive strength of concretes elaborated with these RCA. These results obtained with Raman spectroscopy are very encouraging about the benefits of its implementation to study civil engineering materials. It could cover the hydration stage to alterations they might face once in service (such as external sulfatic attack, corrosion of reinforced bars ...).

References

1. U.S. Geological Survey, 2020, Mineral commodity summaries 2020: U.S. Geological Survey. (2020), 200 p. https://doi.org/10.3133/mcs2020.
2. IPCC report AR6 WGI, Chapter 5: Global Carbon and other Biogeochemical Cycles and Feedbacks (2021).
3. Shagñay S., Bautista A., Velasco F., Torres-Carrasco M. Carbonation of alkali-activated and hybrid mortars manufactured from slag: Confocal Raman microscopy study and impact on wear performance. Boletín de la Sociedad Española de Cerámica y Vidrio. In press (2022). https://doi.org/10.1016/j.bsecv.2022.07.003.
4. Ben Fraj A., Idir R. (2017). Concrete based on recycled aggregates–recycling and environmental analysis: a case study of Paris' region Constr. Build. Mater., 157, pp. 952–964

5. Sedran T. (2019). Chapter 15: Adaptation of existing methods to incorporate recycled aggregates, in: Francois de Larrard, Horacio Colina (Eds.), Concrete Recycling Research and Practice, 1ˢᵗ edition, CRC Press, p. 636 (ISBN 9781138724723).

6. De Larrard F, Colina H. (2019). Concrete recycling: Research and practice. Boca Raton: CRC Press. https://doi.org/10.1201/9781351052825.

7. Zheng Lu, Qihang Tan, Jiali Lin, Dianchao Wang. (2022). Properties investigation of recycled aggregates and concrete modified by accelerated carbonation through increased temperature. Construction and Building Materials, Volume 341, 127813. https://doi.org/10.1016/j.conbuildmat.2022.127813.

8. Yunhui Pu, Lang Li, Xiaoshuang Shi, Qingyuan Wang, Abdelfatah Abomohra. (2022). Improving recycled concrete aggregates using flue gas based on multicyclic accelerated carbonation: Performance and mechanism. Construction and Building Materials, Volume 361, 129623. https://doi.org/10.1016/j.conbuildmat.2022.129623.

9. Chunhua Feng, Buwen Cui, Hui Guo, Wenyan Zhang, Jianping Zhu. (2023). Study on the effect of reinforced recycled aggregates on the performance of recycled concrete--synergistic effect of cement slurry-carbonation. Journal of Building Engineering, Volume 64, 105700. https://doi.org/10.1016/j.jobe.2022.105700.

10. Hui Liu, Xudong Zhu, Pinghua Zhu, Chunhong Chen, Xinjie Wang, Wei Yang, Meirong Zong. (2022). Carbonation treatment to repair the damage of repeatedly recycled coarse aggregate from recycled concrete suffering from coupling action of high stress and freeze-thaw cycles. Construction and Building Materials, Volume 349, 128688. https://doi.org/10.1016/j.conbuildmat.2022.128688.

11. Etxeberria M., Marí A. R., Vázquez E. (2007). Recycled aggregate concrete as structural material. Materials and structures, 40(5), pp.529-541.

12. Silva R. V., De Brito J., Dhir R. K. (2015). The influence of the use of recycled aggregates on the compressive strength of concrete: A review. Eur J Environ Civ Eng., 19, pp. 25-849. https://doi.org/10.1080/19648189.2014.974831

13. Omary S, Ghorbel E, Wardeh G. (2016). Relationships between recycled concrete aggregates characteristics and recycled aggregates concretes properties. Construct Build Mater., 108:163–174. https://doi.org/10.1016/j.conbuildmat.2016.01.042.

14. Bai G., Zhu C., Liu C., Liu B. (2020). An evaluation of the recycled aggregate characteristics and the recycled aggregate concrete mechanical properties. Construction and building materials, 240, 117978.

15. Tošić N., Torrenti J. M., Sedran T., Ignjatović I. (2021). Toward a codified design of recycled aggregate concrete structures: Background for the new fib Model Code 2020 and Eurocode 2. Structural Concrete, 22(5), 2916-2938.

16. Wang B., Yan L., Fu Q., Kasal B. (2021). A comprehensive review on recycled aggregate and recycled aggregate concrete. Resources, Conservation and Recycling, 171, 105565.

17. Damrongwiriyanupap N., Wachum A., Khansamrit K., Detphan S., Hanjtsuwan S., Phoo-ngernkham T., Sukontasukul P. , Li L., Chindaprasirt P. (2022). Improvement of recycled concrete aggregate using alkali-activated binder treatment. Mater Struct 55, 11. https://doi.org/10.1617/s11527-021-01836-1

18. Zhan B., Poon C. S., Liu Q., Kou S. C., Shi C. (2014). Experimental study on CO_2 curing for enhancement of recycled aggregate properties. Constr. Build. Mat., 67, 3–7.

19. Pu Y.; Li L.; Wang Q.; Shi X.; Luan C.; Zhang G.; Fu L.; El-Fatah Abomohra A. (2021). Accelerated carbonation technology for enhanced treatment of recycled concrete aggregates: A state-of-the-art review. Constr. Build. Mat., 282, 122671

20. Zajac M., Skibsted J., Skocek J., Durdzinski P., Bullerjahn F., Ben Haha M. (2020). Phase assemblage and microstructure of cement paste subjected to enforced, wet carbonation. Cement and Concrete Research, 130, 105990, https://doi.org/10.1016/j.cemconres.2020.105990.

21. Li Liang, Min Wu. (2022). An overview of utilizing CO_2 for accelerated carbonation treatment in the concrete industry. Journal of CO_2 Utilization, 60, 102000. https://doi.org/10.1016/j.jcou.2022.102000.

22. Xiao J., Zhang H., Tang Y., Deng Q., Wang D., Poon, C. S. (2022). Fully utilizing carbonated recycled aggregates in concrete: Strength, drying shrinkage and carbon emissions analysis. Journal of Cleaner Production, 377, 134520. https://doi.org/10.1016/j.jclepro.2022.134520.

23. Winnefeld F., Leemann A., German A., Lothenbach B. (2022). CO_2 storage in cement and concrete by mineral carbonation. Current Opinion in Green and Sustainable Chemistry, 100672. https://doi.org/10.1016/j.cogsc.2022.100672.

24. Skocek J., Zajac M., Ben Haha M. (2020). Carbon Capture and Utilization by mineralization of cement pastes derived from recycled concrete. Scientific Reports, 10(1), 1-12. https://doi.org/10.1038/s41598-020-62503-z.

25. Tam V. W., Butera A., Le K. N., Li W. (2020). Utilising CO_2 technologies for recycled aggregate concrete: A critical review. Construction and Building Materials, 250, 118903. https://doi.org/10.1016/j.conbuildmat.2020.118903.

26. Sereng, M.; Djerbi, A.; Metalssi, O.O.; Dangla, P.; Torrenti, J.-M. (2021). Improvement of Recycled Aggregates Properties by Means of CO_2 Uptake. Appl. Sci., 11, 6571. https://doi.org/10.3390/app11146571

27. Jean Michel Torrenti, Ouali Amiri, Laury Barnes-Davin, Frédéric Bougrain, Sandrine Braymand, Bogdan Cazacliu, Johan Colin, Amaury Cudeville, Patrick Dangla, Assia Djerbi, Mathilde Doutreleau, Adelaïde Feraille, Marielle Gueguen, Xavier Guillot, Yunlu Hou, Laurent Izoret, Yvan-Pierre Jacob, Jena Jeong, Jean David Lau Hiu Hoong, Pierre-Yves Mahieux, Jonathan Mai-Nhu, Heriberto Martinez, Vincent Meyer, Vincent Morin, Thomas Pernin, Jean-Marc Potier, Laurent Poulizac, Patrick Rougeau, Myriam Saadé, Lucie Schmitt, Thierry Sedran, Marie Sereng, Anthony Soive, Glaydson Symoes Dos Reys, Philippe Turcry. The FastCarb project: Taking advantage of the accelerated carbonation of recycled concrete aggregates. Case Studies in Construction Materials, volume 17, 2022, e01349. https://doi.org/10.1016/j.cscm.2022.e01349.

28. Mi R., Pan G. (2022a). Inhomogeneities of carbonation depth distributions in recycled aggregate concretes: A visualisation and quantification study, Construction and Building Materials, 330, 127300. https://doi.org/10.1016/j.conbuildmat.2022.127300.

29. Mi R., Liew K. M., Pan G. (2022b). New insights into diffusion and reaction of CO2 gas in recycled aggregate concrete. Cement and Concrete Composites, 129, 104486. https://doi.org/10.1016/j.cemconcomp.2022.104486.

30. Izoret, L., Pernin, T., Potier, J. M., & Torrenti, J. M. (2023). Impact of Industrial Application of Fast Carbonation of Recycled Concrete Aggregates. Applied Sciences, 13(2), 849. https://doi.org/10.3390/app13020849

31. Cole W. F., Kroone B. (1959). Carbonate minerals in hydrated Portland cement, Nature, 184, BA57.

32. Sledgers P. A., Rouxhet P. G. (1976). Carbonation of the hydration products of tricalcium silicate, Cem. Concr. Res., 6, pp. 381–388.

33. Thiery M., Dangla P., Belin P., Habert G., Roussel N. (2013). Carbonation kinetics of a bed of recycled concrete aggregates: A laboratory study on model materials. Cement and Concrete Research, 46, pp. 50-65. https://doi.org/10.1016/j.cemconres.2013.01.005.

34. Auroy M., Poyet S., Le Bescop P., Torrenti J. M., Charpentier T., Moskura M., Bourbon X. (2018). Comparison between natural and accelerated carbonation (3% CO_2): Impact on mineralogy, microstructure, water retention and cracking. Cement and Concrete Research, 109, pp. 64-80. https://doi.org/10.1016/j.cemconres.2018.04.012.

35. Tai, C.Y., and Chen, F.-B. (1998). Polymorphism of CaCO3, precipitated in a constant-composition environment. AIChE Journal, 44, pp. 1790-1798. https://doi.org/10.1002/aic.690440810

36. Drouet E., Poyet S., Le Bescop P., Torrenti, J. M., Bourbon, X. (2019). Carbonation of hardened cement pastes: Influence of temperature. Cement and Concrete Research, 115, pp. 445-459. https://doi.org/10.1016/j.cemconres.2018.09.019.

37. Morandeau, A., Thiery, M., & Dangla, P. (2014). Investigation of the carbonation mechanism of CH and CSH in terms of kinetics, microstructure changes and moisture properties. Cement and Concrete Research, 56, pp. 153-170. https://doi.org/10.1016/j.cemconres.2013.11.015

38. Kaddah F., Ranaivomanana H., Amiri O., Rozière E. (2022). Accelerated carbonation of recycled concrete aggregates: Investigation on the microstructure and transport properties at cement paste and mortar scales. Journal of CO_2 Utilization, 57, 101885.

39. Haque, F., Santos, R. M., Chiang, Y. W. (2019). Using nondestructive techniques in mineral carbonation for understanding reaction fundamentals, Powder Technol., 357, pp. 134-148. https://doi.org/10.1016/j.jcou.2022.101885.

40. Bensted, J. (1976). Uses of Raman spectroscopy in cement chemistry. J. Am. Ceramic Soc. 59 (3-4), pp. 140-143.

41. Bensted, J. (1977). Raman spectral studies of carbonation phenomena, Cement and Concrete Research., 7 (2), pp. 161-164.

42. Kontoyannis C. G., Vagenas N. V. (2000). Calcium carbonate phase analysis using XRD and FT-Raman spectroscopy. Analyst, 125, pp. 251-255. https://doi.org/10.1039/A908609I

43. Martinez-Ramirez S., Sanchez-Cortes S., Garcia-Ramos J. V., Domingo C., Fortes C., Blanco-Varela M. T. (2003). Micro-Raman spectroscopy applied to depth profiles of carbonates formed in lime mortar. Cement and Concrete Research, 33, pp. 2063-2068. https://doi.org/10.1016/S0008-8846(03)00227-8.

44. Renaudin G., Segni R., Mentel D., Nedelec J.-M., Leroux F., Taviot-Gueho C. (2007). A Raman study of the sulfated cement hydrates: ettringite and monosulfoaluminate. Journal of Advanced Concrete Technology, 5, 3, pp. 299-312. https://doi.org/10.3151/jact.5.299.

45. Corvisier J., Brunet F., Fabbri A., Bernard S., Findling N., Rimmelé G., Barlet-Gouédard V., Beyssac O., Goffé B. (2010). Raman mapping and numerical simulation of calcium carbonates distribution in experimentally carbonated Portland cement cores. European Journal of Mineralogy, 22, 1, pp. 63-74. https://doi.org/10.1127/0935-1221/2010/0022-1977.

46. Ševčik R., Mácrová P., Sotiriadis K., Pérez-Estébanez M., Viani A., Šašek P. (2016). Micro-Raman spectroscopy investigation of the carbonation reaction in a lime paste produced with a traditional technology. Journal of Raman Spectroscopy, 47, pp. 1452-1457. https://doi.org/10.1002/jrs.4929.

47. Plank, J., Zhang-Preße, M., Ivleva, N. P., Niessner, R. (2016). Stability of single phase C3A hydrates against pressurized CO_2. Construction and Building Materials, 122, pp. 426-434. https://doi.org/10.1016/j.conbuildmat.2016.06.042.

48. Marchetti M., Mechling J.-M., Diliberto C., Brahim M.-N., Trauchessec R., Lecomte A., Bourson P. (2021). Portable quantitative confocal Raman spectroscopy: non-destructive approach of the carbonation chemistry and kinetics. Cement and Concrete Research, volume 139, pp. 106280. https://doi.org/10.1016/j.cemconres.2021.106554.

49. Marchetti M., Mechling J.-M., Janvier-Badosa S., Offroy M. (2023). Benefits of Chemometric and Raman Spectroscopy Applied to the Kinetics of Setting and Early Age Hydration of Cement Paste, 77, 1, pp. 37-52. https://doi.org/10.1177/00037028221135065.

50. Srivastava S., Garg N. (2023). Tracking spatiotemporal evolution of cementitious carbonation via Raman imaging. Journal of Raman Spectroscopy, 54, 4, pp. 414-425. https://doi.org/10.1002/jrs.6483.

51. Zhang, B., Liao, W., Ma, H., Huang, J. (2023). In situ monitoring of the hydration of calcium silicate minerals in cement with a remote fiber-optic Raman probe. Cement and Concrete Composites, 142, 105214. https://doi.org/10.1016/j.cemconcomp.2023.105214.

52. Brahim M.-N., Mechling J.-M., Janvier-Badosa S., Marchetti M. (2023). Early stage ettringite and monosulfoaluminate carbonation investigated by in situ Raman spectroscopy coupled with principal component analysis, Materials Today Communications, 105539. https://doi.org/10.1016/j.mtcomm.2023.105539.

53. Xue, Q., Zhang, L., Mei, K., Wang, L., Wang, Y., Li, X., Cheng, X., Liu, H. (2022). Evolution of structural and mechanical properties of concrete exposed to high concentration CO_2. Construction and Building Materials, 343, 128077. https://doi.org/10.1016/j.conbuildmat.2022.128077.

54. Djerbi A. (2018). Effect of recycled coarse aggregate on the new interfacial transition zone concrete. Construction and Building Materials, 190, pp. 1023-1033. https://doi.org/10.1016/j.conbuildmat.2018.09.180.

55. Richardson, I. G., Skibsted, J., Black, L., Kirkpatrick, R. J. (2010). Characterisation of cement hydrate phases by TEM, NMR and Raman spectroscopy. Advances in Cement Research, 22 (4), pp. 233-248. https://doi.org/10.1680/adcr.2010.22.4.233.

56. Martínez-Ramírez S., Fernández-Carrasco L. (2012). Carbonation of ternary cement systems. Construction and Building Materials, 27, 1, pp. 313-318. https://doi.org/10.1016/j.conbuildmat.2011.07.043.

57. Martínez-Ramírez S., Gutierrez-Contreras R., Husillos-Rodriguez N., Fernández-Carrasco L. (2016). In-situ reaction of the very early hydration of C3A-gypsum-sucrose system by Micro-Raman spectroscopy. Cement and Concrete Composites, 73, pp. 251-256. https://doi.org/10.1016/j.cemconcomp.2016.07.020.

58. Mi T., Li Y., Liu W., Li W., Long W., Dong Z., Gong Q., Xing F., Wang Y. (2021). Quantitative evaluation of cement paste carbonation using Raman spectroscopy. npj Mater Degrad 5, 35. https://doi.org/10.1038/s41529-021-00181-6

59. Wehrmeister U., Soldati A. L., Jacob D. E., Häger, T., Hofmeister, W. (2010), Raman spectroscopy of synthetic, geological and biological vaterite: a Raman spectroscopic study. J. Raman Spectrosc., 41: 193-201. https://doi.org/10.1002/jrs.2438

60. Ševčík R., Mácová P. (2018). Localized quantification of anhydrous calcium carbonate polymorphs using micro-Raman spectroscopy. Vibrational Spectroscopy, volume 95, pp. 1-6. https://doi.org/10.1016/j.vibspec.2017.12.005.

61. Kramer K. (1988). Chemiometric Techniques for Quantitative Analysis; CRC Press.

62. Jackson J. E. (2003). A User's Guide to Principal Components; John Wiley & Sons.

63. Brereton, R. G. (2003). Chemometrics: Data Analysis for the Laboratory and chemical Plant; John Wiley & Sons, Ltd.

64. Brereton R. G. (2007) Applied Chemometrics for Scientists; John Wiley & Sons, Ltd.

65. Ruckebusch C. (2016). Data Handling in Science and Technology, Volume 30 Resolving spectral mixtures; Elsevier

66. Offroy, M., Moreau, M., Sobanska, S., Milanfar, P., Duponchel, L. (2015). Pushing back the limits of Raman imaging by coupling super-resolution and chemometrics for aerosols characterization. Scientific Reports, 5, 12303. DOI: 10.1038/srep1230.

67. Haouchine M., Biache C., Lorgeoux C., Faure P., Offroy M. (2022). Handle Matrix Rank Deficiency, Noise, and Interferences in 3D Emission-Excitation Matrices: Effective Truncated Singular-Value Decomposition in Chemometrics Applied to the Analysis of

Polycyclic Aromatic Compounds. ACS Omega, 7 (27), pp. 23653-23661. DOI: 10.1021/acsomega.2c02256

68. Windig W., Guilment J. (1991). Interactive self-modeling mixture analysis. Anal. Chem., 63, 1425-1432. DOI: 10.1021/ac00014a016.

69. Windig W., Stephenson D. (1992). Self-modeling mixture analysis of second-derivative near-infrared spectral data using the SIMPLISMA approach. A. Anal. Chem., 64, 2735-2742. DOI: 10.1021/ac00046a015.

70. Sánchez F. C., Van Den Bogaert B., Rutan S., Massart D. L. (1996). Multivariate peak purity approaches. Chemom. Intell. Lab. Syst., 34, pp. 139-171. https://doi.org/10.1016/0169-7439(96)00020-2.

71. Urmos J., Sharma S. K., Mackenzie F. T. (1991). Characterization of some biogenic carbonates with Raman spectroscopy. American Mineralogist, 76, pp. 641-646.

72. Gauldie R. W., Sharma S. K., Volk E. (1997). Micro-Raman Spectral Study of Vaterite and Aragonite Otoliths of the Coho Salmon, Oncorhynchus kisutch. Camp, Biochem. Physiol., volume 118A, 3, pp. 753-757. https://doi.org/10.1016/S0300-9629(97)00059-5.

73. Gabrielli, C., Jaouhari, R., Joiret, S. and Maurin, G. (2000), In situ Raman spectroscopy applied to electrochemical scaling. Determination of the structure of vaterite. J. Raman Spectrosc., 31, pp. 497-501. https://doi.org/10.1002/1097-4555(200006)31:6<497::AID-JRS563>3.0.CO;2-9

74. Kontoyannis C. G., Vagenas N. V. (2000). Calcium carbonate phase analysis using XRD and FT-Raman spectroscopy. Analyst, 125, pp. 251-255. https://doi.org/10.1039/A908609I.

75. Garbev K., Stemmermann P., Black L., Breen C., Yarwood J., Gasharova B. (2007). Structural features of C-S-H(I) and its carbonation in air - a Raman spectroscopic study. Part I: fresh phases, J. Am. Soc., 90 (3), pp. 900–907. https://doi.org/10.1111/j.1551-2916.2006.01428.x.

76. Black L., Breen C., Yarwood J., Garbev K., Stemmermann P., Gasharova B. (2007). Structural features of C-S-H(I) and its carbonation in air - a Raman spectroscopic study. Part II: carbonated phases, J. Am. Soc., 90 (3), pp. 908–917. https://doi.org/10.1111/j.1551-2916.2006.01429.x

77. Soldati A. L., Jacob D. E., Wehrmeister U., Hofmeister W. (2008). Structural characterization and chemical composition of aragonite and vaterite in freshwater cultured pearls. Mineralogical Magazine, volume 72, 2, pp. 579–592. https://doi.org/10.1180/minmag.2008.072.2.579.

78. Cruz J. A., Sánchez-Pastor N., Gigler A. M., Fernández-Díaz L. (2011). Vaterite Stability in the Presence of Chromate, Spectroscopy Letters, 44, 7-8, pp. 495-499. http://dx.doi.org/10.1080/00387010.2011.610408

79. De La Pierre M., Carteret C., Maschio L., André E., Orlando R., Dovesi R. (2014). The Raman spectrum of $CaCO_3$ polymorphs calcite and aragonite: A combined experimental and computational study. J. Chem. Phys., 140, 164509. https://doi.org/10.1063/1.4871900

80. Donnelly F. C., Purcell-Milton F., Framont V., Cleary O., Dunne P. W., Gun'ko Y. K. (2017). Synthesis of $CaCO_3$ nano- and micro-particles by dry ice carbonation. Chem. Commun., 53, 6657. https://doi.org/10.1039/C7CC01420A.

81. Yue Y., Wang J. J., Muhammed Basheer P. A., Boland J. J., Bai Y. (2017). Characterisation of carbonated Portland cement paste with optical fibre excitation Raman spectroscopy. Construction and Building Materials, 135, pp. 369-376. https://doi.org/10.1016/j.conbuildmat.2017.01.008.

82. Yue Y., Wang J. J., Muhammed Basheer P. A., Boland J. J., Bai Y. (2018). A Raman spectroscopy based optical fibre system for detecting carbonation profile of cementitious

materials. Sensors and Actuators B: Chemical, 257, pp. 635-649. https://doi.org/10.1016/j.snb.2017.10.160.

305
306
307
308